Journal of Electronics and Electrical Engineering
https://ojs.wiserpub.com/index.php/JEEE

Research Article

Research on The Frequency Response Characteristics Calculation of Z-Type Transformer Winding Based on A Decomposition Algorithm

Zirui Liu[1], Binyu Zhu[1], Huan Peng[1], Zhenlin Yuan[1], Song Wang[1,2*], Jun Liu[2]

[1] Department of Power and Electrical Engineering, Northwest A&F University, Yangling 712100, China
[2] Hangzhou Qiantang River Electric Group Co., Ltd, Hangzhou 311200, China
[*] Correspondence: sw@nwafu.edu.cn

Received: 16 April 2026; **Revised:** 2 June 2026; **Accepted:** 3 June 2026; **Published:** 22 June 2026

Abstract: To enhance the computational efficiency of frequency response for Z-type transformer windings with complex structures, an efficient decomposition algorithm for frequency response calculation is proposed, focusing on a lightning protection transformer with Yzn11 connection type. First, considering the structural characteristics of the equivalent circuit of the transformer winding, the equivalent circuit model is decomposed into three decoupled sub-networks. Then, the branch admittance matrices and incidence matrices of each sub-network are calculated. Subsequently, based on the interconnection relationships among the sub-networks within the entire network, the global nodal admittance matrix is constructed to establish a decomposition algorithm for frequency response analysis of the equivalent circuit of the Z-type transformer winding. Furthermore, the accuracy of the proposed method is verified with PSpice circuit simulation software. Finally, the superiority of the algorithm in terms of computation time is demonstrated by comparison with the traditional node voltage method. The results show that in terms of accuracy, the frequency response curves (six sets) of high- and low-voltage windings for phases A, B, and C obtained by the proposed method almost completely overlap with those simulated by PSpice. The correlation coefficients are larger than 0.999, and the comparative standard deviations are less than 0.7. The proposed method is superior to the traditional node voltage method in terms of computational efficiency. Especially, as the number of discs increases to 100, the computation time of the proposed method is reduced by 55.3%, and the calculation efficiency is significantly improved.

***Keywords*:** transformer, Z-type transformer, decomposition algorithm, frequency response, equivalent circuit

1. Introduction

The Z-type transformer features a special winding structure in which each phase winding on the iron core is divided into two sections and connected in series with reverse polarity to form a star connection. This configuration provides excellent lightning protection performance and flexible neutral-point grounding capability. It effectively suppresses inverse transformation overvoltage during single-phase grounding faults and reduces neutral-point unbalanced current under normal operation. Consequently, Z-type transformers are widely used as lightning protection and grounding transformers in mining areas, industrial sensitive loads, and other special power supply scenarios [1, 2].

Despite these advantages, the winding remains one of the most critical internal components, and its deformation becomes increasingly severe as the system's short-circuit level rises. Therefore, reliable winding deformation detection

DOI: https://doi.org/10.37256/jeee.5120269933

for Z-type transformers is essential. Wang et al. [3] developed a magnetic-structural coupling model for cumulative deformation analysis of transformer windings under short-circuit faults, revealing the mechanical stress distribution in windings. Zhang et al. [4] further extended this work using 3-D finite element methods to analyze cumulative deformation, providing deeper insights into the mechanical behavior of transformer windings under fault conditions. Frequency Response Analysis (FRA), as a non-destructive and highly sensitive transformer winding deformation detection method, has been widely used in the deformation diagnosis of power equipment [5]. The IEEE Std C57.149-2024 [6] provides comprehensive guidance on the application and interpretation of Frequency Response Analysis for oil-immersed transformers, while Al-Ameri et al. [7] presented detailed interpretation methods for fault detection using FRA. Amara et al. [8] developed a novel auto-synthesis method to construct high-frequency equivalent circuits of transformer windings based on signal morphology interpretation of FRA data, enabling automated parameter identification from frequency sub-bands. Saji et al. [9] estimated the effect of axial displacement on equivalent circuit parameters of transformer windings using finite element method and analyzed its impact on sweep frequency response signatures. Samimi and Tenbohlen [10] provided a comprehensive state-of-the-art review on FRA interpretation using numerical indices, standardizing the evaluation criteria for FRA results. This method compares and analyzes the differences between the curves by measuring the FRA curve of the transformer winding in the healthy and fault states. In order to deeply explore the relationship between the deformation state of the transformer winding and the frequency response, establishing an equivalent circuit model of the transformer winding and calculating its FRA curve has become a key step in using simulation methods to study transformers [11].

Up to now, a large number of scholars have devoted themselves to the frequency response calculation method of traditional power transformer winding equivalent circuits. Nguyen and Pham [12] proposed a frequency response calculation method for the equivalent circuit of power transformers based on a state-space model. The method avoids symbolic calculations to reduce computational complexity. However, the method still requires the independent state variables to be screened out in advance, and the calculation process remains complicated. In the literature [13] the performance differences between Nodal Voltage Matrix method (NVM) and State Space Method (SSM) in the calculation of FRA curves of double winding transformers are directly compared. The research shows that the node voltage matrix method is simpler in implementation. Wang et al. [14] proposed cut-set matrix methods for Frequency Response Analysis curves of lumped parameter equivalent circuit model of three-winding power transformers. Without selecting a tree, the process is simpler, and the calculation efficiency is better than the traditional node method, providing an efficient matrix-based approach for FRA calculation. Ren et al. [15] proposed a low-order algorithm that only requires two matrix inverses for frequency response calculation of transformer equivalent circuits, significantly reducing computational complexity. In the literature [16], the transfer function obtained from FRA data can be employed to derive the transformer winding equivalent circuit, providing a systematic approach for parameter identification and circuit modeling. In summary, although the above research has made some progress, the above research is aimed at the traditional single-phase double-winding transformer. It does not consider the situation of three-phase and the problem of three-phase connection groups, nor does it involve Z-type three-phase transformers with a two-stage, anti-polar series connection structure. However, for this kind of transformer with complex structure and connection, using traditional circuit algorithms to solve the frequency response, it is necessary to directly construct a high-dimensional equation system containing the information of the entire branch line and node network, resulting in an exponential increase in computational complexity, and it is difficult to meet the high-efficiency frequency response calculation needs of Z-type transformers.

To address this challenge, this paper takes a typical Z-type lightning protection transformer with Yzn11 connection group as an example to develop an efficient frequency response calculation method for its winding equivalent circuit. First, according to the structural characteristics of Z-type transformer, the lumped parameter equivalent circuit model including three-phase winding self inductance, mutual inductance, ground capacitance and parallel capacitance between windings is established, and the systematic numbering rules of nodes and branches are formulated to meet the requirements of the matching algorithm. Second, based on the coupling relationships among components in the whole equivalent circuit network, a division strategy is proposed to construct three uncoupled subnetworks. Third, use the circuit principle to calculate the branch inductance matrix and correlation matrix of each subnetwork respectively. Furthermore, an overall node inductance matrix is built according to the positional relationship of each subnetwork within the whole network, leading to a Z-type winding FRA decomposition algorithm. Finally, the correctness of the method is verified using

PSpice circuit simulation software, and its computational efficiency advantage over the traditional node voltage method is demonstrated through comparison.

2. Basic principles

2.1 *Structural characteristics and working principle of Z-type transformers*

The structure of Z-type transformer is the same as that of ordinary three-phase core power transformer. The difference is that each phase winding is equally divided into two sections, and the two sections on different iron cores are connected in reverse series to form a phase winding, and the three-phase ends are connected into a zigzag connection. Its structure and winding connection are shown in Figure 1.

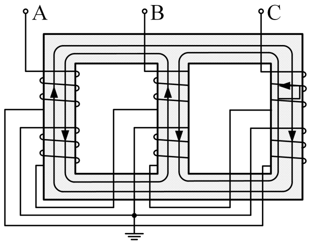

Figure 1. Z-type transformer structure and winding connection diagram

Among Z-type transformers, lightning protection transformers with the connection group Yzn11 are the most widely used. Therefore, this paper takes this transformer as an example for analysis and calculation. The connection diagram and phase diagram of the Yzn11 connection group are shown in Figure 2.

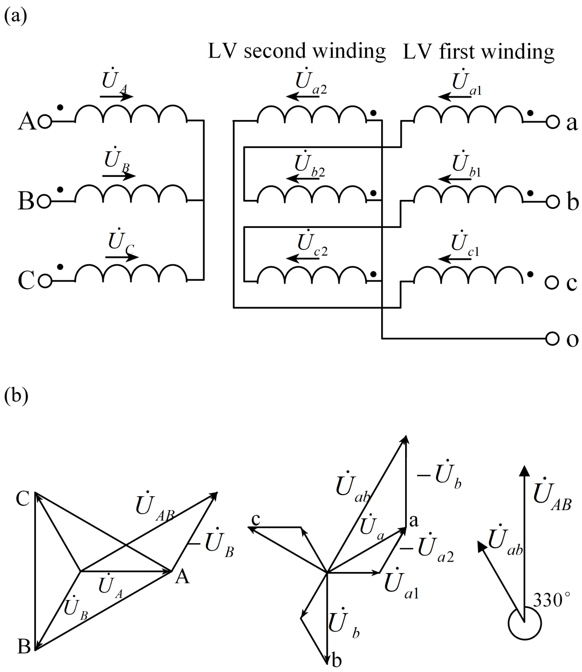

Figure 2. Yzn11 connection group connection diagram and phase relationship diagram. (a) Yzn11 transformer high-voltage and low-voltage winding connection diagram; (b) Yznl1 connection group vector diagram

In this type of transformer, when lightning strikes the high-voltage side, the residual voltage generated by the surge arrester is applied to the neutral point of the low-voltage winding. Since there are two windings on the same iron core column on the low-voltage side, the induced electromotive forces of the two windings cancel each other out, and no overvoltage will occur. Similarly, when lightning strikes the low-voltage side, the lightning current can flow through the three-phase windings simultaneously and ground, so that the zero-sequence magnetic flux generated on each iron core column is equal in magnitude and opposite in direction, and the total magnetic flux is zero, and the overvoltage will not be induced on the high-voltage side line [17, 18].

2.2 *Basic principles of FRA*

FRA is a non-destructive testing method that uses a low-voltage, sinusoidal sweep frequency signal as input. By calculating the amplitude of the response voltage and the input voltage over the entire frequency band, the frequency response amplitude data can be obtained [19]. By plotting the relationship curve between the frequency response amplitude and all frequency points, the FRA curve reflecting the winding state can be obtained. By comparing the changes in the FRA curve before and after the fault, the fault state of the winding can be evaluated.

The formula for calculating the frequency response amplitude data of the winding is [20]:

$$\mathrm{FRA}_{\mathrm{magnitude}} = 20 * \lg \left| \frac{U_o(\omega)}{U_i(\omega)} \right|, \tag{1}$$

where U_o and U_i are the response voltage and the injected wide-bandwidth sinusoidal sweep frequency voltage signal (1 kHz–1 MHz), respectively, measured at the two ends of the transformer winding.

3. Equivalent circuit modeling of Z-type lightning protection transformer

Based on the fundamental principles of FRA, the windings of a three-phase lighting protection transformer with connection group Yzn11 can be equivalently represented as a passive linear two-port network. Using a single disc as a unit, an equivalent circuit for a Z-type transformer is established, as shown in Figure 3. The model consists of n (even number) coil units, including the self-inductances L_{sh} and L_{sl} of the high/low voltage windings; the mutual inductances M_{sh}, M_{sl}, and M_{hl} between coils; the series resistances R_{sh} and R_{sl} of the high/low voltage windings; the series capacitances C_{sh} and C_{sl}; the capacitances to ground C_{gh} and C_{gl}; the parallel capacitance C_{hl} between the high and low voltage windings; and the parallel capacitances C_{AB} and C_{BC} between adjacent high-voltage windings.

To achieve consistency and programmability in node and branch numbering, the following numbering rules are adopted: Nodes are numbered sequentially from low-voltage to high-voltage windings. The low-voltage three phases a, b, and c are assigned nodes 1~n, $n + 1$~$2n$, and $2n + 1$~$3n$ respectively. The neutral point of the low-voltage winding is led out through node $3n + 1$. The high-voltage three phases A, B, and C are numbered $3n + 2$~$4n + 1$, $4n + 2$~$5n + 1$, and $5n + 2$~$6n + 1$ respectively. The ends of the high-voltage three phases converge at node $6n + 2$ to form a star connection. Since the low-voltage winding is divided into a first winding and a second winding from the middle position, as shown in Figure 2a, and the ends of the first windings of low-voltage phases a, b, and c are connected to the ends of the second windings of low-voltage phases b, c, and a respectively, the connected nodes share the same number, which is $0.5n + 1$, $1.5n + 1$, and $2.5n + 1$ respectively.

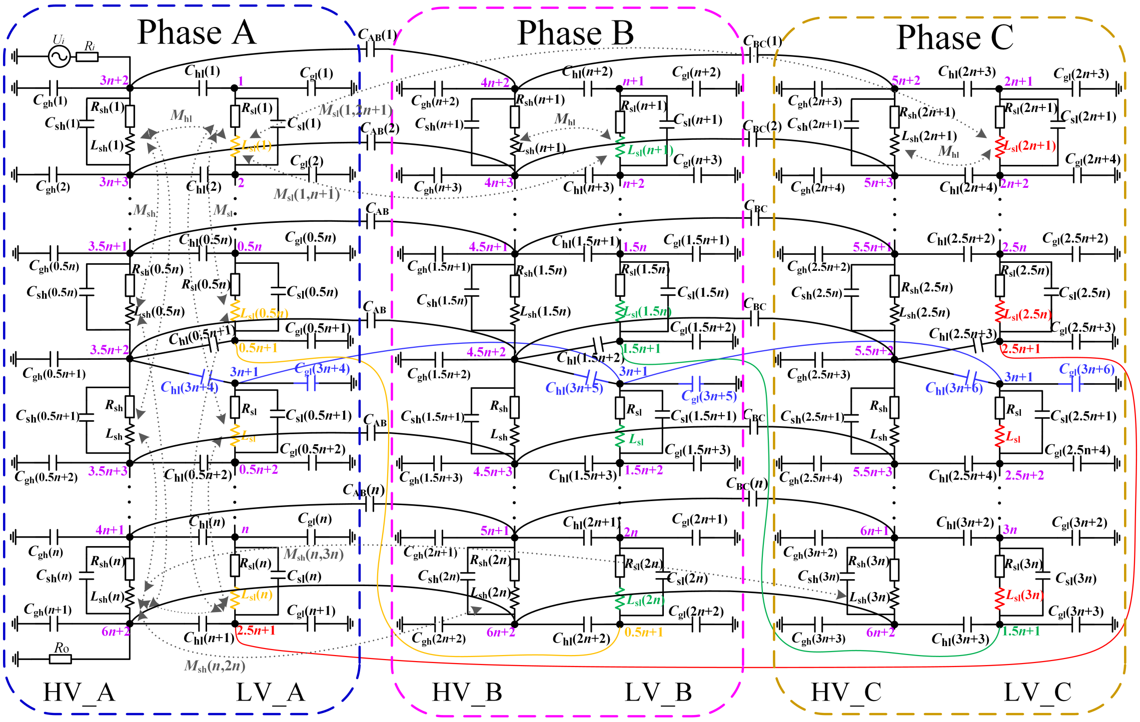

Figure 3. Lumped parameter equivalent model of Yzn11 transformer

4. Establishment of equivalent circuit decomposition algorithm

4.1 *Establishment of generalized branches*

Based on the branch characteristics of the equivalent circuit of the transformer winding lumped parameters in Figure 3, the corresponding generalized branches in the complex frequency domain are constructed [21], as shown in Figure 4.

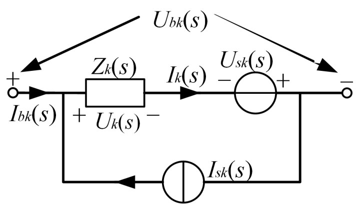

Figure 4. Generalized branch in the complex frequency domain

Based on the voltage and current relationship in Figure 4, we can obtain:

$$U_{bk}(s) = Z_k(s)\left[I_{bk}(s) + I_{sk}(s)\right] - U_{sk}(s). \tag{2}$$

Here, $U_{bk}(s)$ and $I_{bk}(s)$ are the voltage and current transform functions of the branch, respectively, and $Z_k(s)$ is the complex frequency domain impedance of the branch. $U_k(s)$ and $I_k(s)$ are the voltage and current transform functions of the passive components, while $U_{sk}(s)$ and $I_{sk}(s)$ denote the voltage transform function of the independent voltage source and the current transform function of the independent current source, respectively.

By writing the Voltage-Current Relationship (VCR) equations for all branches in the equivalent circuit of the transformer winding and arranging them in matrix form, we obtain

$$\mathbf{U}_b(s) = \mathbf{Z}_b(s)\mathbf{I}_b(s) + \mathbf{Z}_b(s)I_s(s) - U_s(s), \tag{3}$$

where $\mathbf{U}_b(s)$, $\mathbf{I}_b(s)$, and $\mathbf{Z}_b(s)$ are the branch voltage matrix, branch current matrix, and branch impedance matrix of the equivalent circuit, respectively.

When $\mathbf{Z}_b$ is full rank, the branch impedance matrix $\mathbf{Z}_b$ has an inverse matrix $\mathbf{Y}_b$, that is, equation (3) can be transformed into:

$$\mathbf{I} = \mathbf{Y}_b\left(\mathbf{U} - \mathbf{U}_s\right) + \mathbf{I}_s, \tag{4}$$

where $\mathbf{Y}_b$ is the branch admittance matrix, and $\mathbf{Y}_b$, $\mathbf{I}$ and $\mathbf{U}$ are the branch current and branch voltage column vectors, respectively. $\mathbf{I}_s$ and $\mathbf{U}_s$ are the current source and voltage source vectors.

According to the principle of Frequency Response Analysis, the input is a known voltage source, but does not include current sources. Therefore, the current source column vector can be discarded, and the above equation can be further simplified to:

$$\mathbf{I} = \mathbf{Y}_b\left(\mathbf{U} - \mathbf{U}_s\right). \tag{5}$$

4.2 *Establishment of the equivalent circuit equation matrix*

The KCL and KVL equations represented by the correlation matrix $\mathbf{A}$ are as follows [22]:

$$\begin{cases} \mathbf{AI} = 0 \\ \mathbf{A}^T\mathbf{U}_n = \mathbf{U} \end{cases}, \tag{6}$$

where $\mathbf{A}$ is the correlation matrix, $\mathbf{U}_n$ is the node voltage vector, and $\mathbf{U}$ is the branch voltage column vector.

The row number of matrix $\mathbf{A}$ corresponds to the node number, and the column number corresponds to the branch number. The element a_{ij} in the ith row and jth column of the matrix is a_{ij} defined as

$$a_{ij} = \begin{cases} 1, & \text{branch } j \text{ flows out from node } i \\ -1, & \text{branch } j \text{ flows into node } i \\ 0, & \text{branch } j \text{ is not connected to node } i \end{cases}. \tag{7}$$

Substituting the branch equation (5) into (6), we can obtain

$$\mathbf{AY}_b\mathbf{A}^T\mathbf{U}_n = \mathbf{AY}_b\mathbf{U}_s. \tag{8}$$

Let

$$\mathbf{Y}_n = \mathbf{A}\mathbf{Y}_b\mathbf{A}^T, \tag{9}$$

$$\mathbf{J}_n = \mathbf{A}\mathbf{Y}_b\mathbf{U}_s. \tag{10}$$

Equation (8) can be simplified to

$$\mathbf{U}_n = \mathbf{Y}_n^{-1}\mathbf{J}_n, \tag{11}$$

where $\boldsymbol{Y}_n$ is the equivalent nodal admittance matrix, and $\mathbf{J}_n$ is the equivalent current column vector injected into each node.

4.3 *Calculation of node voltage vectors*

To improve computational efficiency and avoid directly writing high-dimensional equations for this complex network, the network is decomposed at the nodes. All independent nodes of the equivalent circuit are selected as the node set N = {1, 2, …, $6n + 2$}, and the original network is decomposed into three topologically independent subnetworks: Subnetwork 1, containing inductance (including self-inductance and mutual inductance) and parallel capacitance branches; and Subnetwork 2, containing low-voltage winding capacitance, and Subnetwork 3, containing high-voltage winding capacitance, respectively. Network segmentation is achieved through the branch set B = $B_1 \cup B_2 \cup B_3$, where B_1 represents the branch set of the inductance subnetwork, and B_2 and B_3 correspond to the branch sets of the low-voltage and high-voltage winding capacitance, respectively. Since there is no coupling between the subnetworks, and no coupling effect within subnetworks 2 and 3, the computational complexity can be effectively reduced while maintaining system integrity. Regarding branch numbering, a priority order was established for the three electrical networks: inductance branches first, then capacitance branches; low-voltage windings first, then high-voltage windings; and numbering sequentially from phase A to phase C. The capacitor branches within each sub-network are arranged in a specific sequence: sub-network 1 follows the sequence C_{hl}, C_{AB}, C_{BC}; sub-network 2 follows C_{gl} then C_{sl}; and sub-network 3 follows C_{sh} then C_{gh}. To optimize the program architecture, the C_{hl} and C_{gl} leading from the neutral terminal of the three-phase low-voltage windings are uniformly placed at the end of their respective categories. Statistical analysis shows that the total number of branches for sub-networks 1, 2, and 3 are $11n + 6$, $6n + 6$, and $6n + 5$, respectively.

4.3.1 *Sub-network 1 containing inductance and parallel capacitance*

Sub-network 1, as shown in Figure 5, contains the low-voltage inductance L_{sl}, the high-voltage inductance L_{sh}, the high-low voltage parallel capacitance C_{hl}, and the parallel capacitance C_{AB} and C_{BC} between adjacent high-voltage phases in phases A, B, and C. Grouping all inductance into subnetwork 1 allows the self-inductance and mutual inductance elements in the entire inductance matrix to be concentrated together, making programming and solving easier [23]. The branch set of subnet 1 is B_1 = {1, 2, ..., $11n + 6$}.

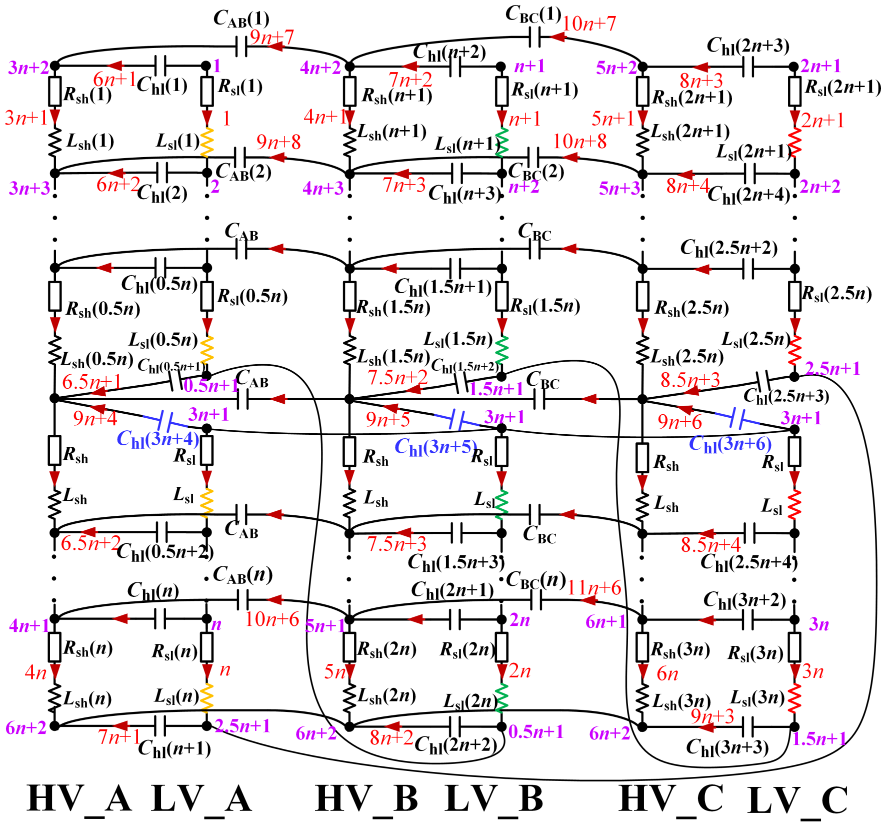

Figure 5. Subnet 1

According to the numbering order of each branch in subnetwork 1 in Figure 5, the branch impedance matrix with dimension $(11n + 6) \times (11n + 6)$ can be obtained as follows:

$$\mathbf{Z}_{b1} = \begin{bmatrix} \mathbf{Z}_{LRM} & 0 \\ 0 & \mathbf{Z}_{C} \end{bmatrix}, \tag{12}$$

where $\mathbf{Z}_{LRM}$ is the impedance matrix composed of the self-inductance, resistance, and mutual inductance between the series inductance branches of the high and low voltage windings [24], as shown in Equation (13). $\mathbf{Z}_C$ is the impedance matrix of each capacitance branch in subnetwork 1, as shown in Equation (19).

$$\mathbf{Z}_{LRM} = \begin{bmatrix} s\mathbf{L}_L + \mathbf{R}_L & \mathbf{M}_{LH} \\ \mathbf{M}_{HL} & s\mathbf{L}_H + \mathbf{R}_H \end{bmatrix}, \tag{13}$$

where $\mathbf{L}_H$ and $\mathbf{L}_L$ are the self-inductance matrices of the high and low voltage windings of the three phases, respectively, both of which are diagonal matrices, as shown in Equations (14) and (15). $\mathbf{M}_{LH}$ and $\mathbf{M}_{HL}$ are the mutual inductance matrices between the high and low voltage windings of the three phases, $\mathbf{M}_{LH} = \mathbf{M}_{HL}^T$, as shown in Equation (16). $\mathbf{R}_H$ and

$\mathbf{R}_L$ are the resistance matrices of the high and low voltage windings of the three phases, respectively, both of which are diagonal matrices, as shown in Equations (17) and (18).

$$\mathbf{L}_H = \begin{bmatrix} L_{sh}(1) & M_{sh}(1,2) & L & M_{sh}(1,3n) \\ M_{sh}(2,1) & L_{sh}(2) & L & M_{sh}(2,3n) \\ M & M & O & M \\ M_{sh}(3n,1) & M_{sh}(3n,2) & L & L_{sh}(3n) \end{bmatrix} \tag{14}$$

$$\mathbf{L}_L = \begin{bmatrix} L_{sl}(1) & M_{sl}(1,2) & L & M_{sl}(1,3n) \\ M_{sl}(2,1) & L_{sl}(2) & L & M_{sl}(2,3n) \\ M & M & O & M \\ M_{sl}(3n,1) & M_{sl}(3n,2) & L & L_{sl}(3n) \end{bmatrix} \tag{15}$$

$$\mathbf{M}_{HL} = \begin{bmatrix} M_{hl}(1,1) & L & M_{hl}(1,3n) \\ M & O & M \\ M_{hl}(3n,1) & L & M_{hl}(3n,3n) \end{bmatrix} \tag{16}$$

$$\mathbf{R}_H = \mathrm{diag}(R_{sh}(1), R_{sh}(2), \ldots, R_{sh}(n), \ldots, R_{sh}(3n)) \tag{17}$$

$$\mathbf{R}_L = \mathrm{diag}(R_{sl}(1), R_{sl}(2), \ldots, R_{sl}(n), \ldots, R_{sl}(3n)) \tag{18}$$

$$\mathbf{Z}_C = \begin{bmatrix} 1/s\ \mathbf{C}_{hl} & 0 & 0 \\ 0 & 1/s\ \mathbf{C}_{AB} & 0 \\ 0 & 0 & 1/s\ \mathbf{C}_{BC} \end{bmatrix}, \tag{19}$$

where $\boldsymbol{C}_{\mathrm{hl}}$ is the parallel capacitance matrix between the high and low voltage windings of the three phases, as shown in equation (20). $\boldsymbol{C}_{\mathrm{AB}}$ and $\boldsymbol{C}_{\mathrm{BC}}$ are the parallel capacitance between the high voltage windings of phase A and phase B, and phase B and phase C, respectively, as shown in equations (21) and (22).

$$\mathbf{C}_{hl} = \mathrm{diag}(C_{hl}(1), C_{hl}(2), \ldots, C_{hl}(3n+6)), \tag{20}$$

$$\mathbf{C}_{AB} = \mathrm{diag}(C_{AB}(1), C_{AB}(2), \ldots, C_{AB}(n)), \tag{21}$$

$$\mathbf{C}_{BC} = \mathrm{diag}(C_{BC}(1), C_{BC}(2), \ldots, C_{BC}(n)). \tag{22}$$

The correlation matrix $\mathbf{A}_1$ corresponding to subnetwork 1 can be obtained according to the relationship between the node number and branch direction in Figure 5, according to formula (7). The dimension of A1 is $(6n+2) \times (11n+6)$.

4.3.2 *Subnet 2 containing low-voltage winding capacitance*

Subnet 2, as shown in Figure 6, contains the three-phase low-voltage to-ground capacitance C_{gl} and the longitudinal capacitance C_{sl}. The branch set $B_2 = \{1, 2, \ldots, 6n+6\}$.

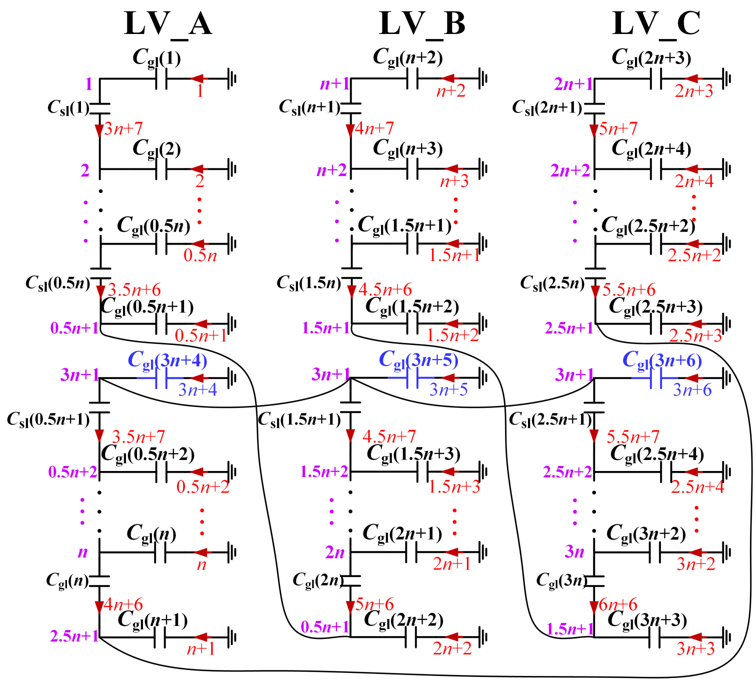

Figure 6. Subnet 2

According to the branch numbering order of this network, the subnet branch impedance matrix $\mathbf{Z}_{b2}$ with dimension $(6n+6) \times (6n+6)$ can be obtained as:

$$\mathbf{Z}_{b2} = \begin{bmatrix} 1/sC_{gl} & 0 \\ 0 & 1/sC_{sl} \end{bmatrix}, \tag{23}$$

where $\mathbf{C}_{gl}$ and $\mathbf{C}_{sl}$ are shown in equations (24) and (25).

$$\mathbf{C}_{gl} = \mathrm{diag}(C_{gl}(1), C_{gl}(2), \ldots, C_{gl}(3n+6)), \tag{24}$$

$$\mathbf{C}_{sl} = \mathrm{diag}(C_{sl}(1), C_{sl}(2), \ldots, C_{sl}(3n)). \tag{25}$$

The correlation matrix $\mathbf{A}_2$ of this subnetwork is calculated in the same way as $\boldsymbol{A}_1$, and its dimension is $(3n + 1) \times (6n + 6)$.

4.3.3 *Subnetwork 3 containing high-voltage winding capacitance*

Subnetwork 3, as shown in Figure 7, contains the three-phase high-voltage-to-ground capacitance C_{gh}, longitudinal capacitance C_{sh}, input resistance R_i, and output resistance R_{o}. The branch set $\text{B}_3 = \{1, 2, \ldots, 6n + 5\}$.

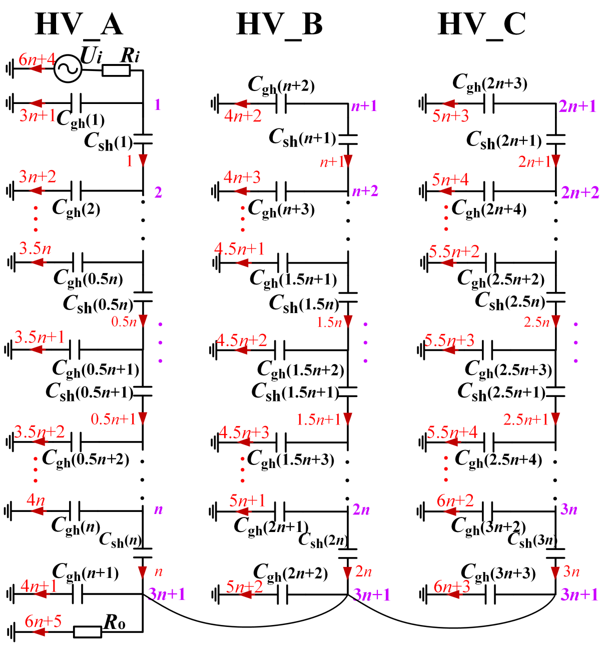

Figure 7. Subnet 3

The branch impedance matrix of subnetwork 3 is shown as:

$$\mathbf{Z}_{b3} = \text{diag}\left(\frac{1}{s\mathbf{C}_{sh}}, \frac{1}{s\mathbf{C}_{gh}}, R_i, R_o\right), \tag{26}$$

where $\boldsymbol{C}_{\text{sh}}$ and $\boldsymbol{C}_{\text{gh}}$ represent the longitudinal capacitance matrix and ground capacitance matrix of the three-phase high-voltage winding, respectively. They are shown as:

$$\mathbf{C}_{sh} = \text{diag}\left(C_{sh}(1), C_{sh}(2), \ldots, C_{sh}(3n)\right), \tag{27}$$

$$\mathbf{C}_{gh} = \text{diag}\left(C_{gh}(1), C_{gh}(2), \ldots, C_{gh}(3n+6)\right). \tag{28}$$

Similarly, the method for obtaining the correlation matrix $\mathbf{A}_3$ of this network is the same as that for the correlation matrix of the subnetwork described above. Here, the dimension of $\mathbf{A}_3$ is $(3n + 1) \times (6n + 5)$.

4.3.4 *Aggregation of the three sub-networks*

The branch impedance matrices $\boldsymbol{Z}_{b1}$, $\boldsymbol{Z}_{b2}$ and $\boldsymbol{Z}_{b3}$ of the three sub-networks are inverted to obtain the branch admittance matrices $\boldsymbol{Y}_{b1}$, $\boldsymbol{Y}_{b2}$ and $\boldsymbol{Y}_{b3}$ of each sub-network. Then, the branch admittance matrices and their corresponding correlation matrices $\boldsymbol{A}_1$, $\boldsymbol{A}_2$ and $\boldsymbol{A}_3$ are substituted into equation (9) to calculate the nodal admittance matrices $\boldsymbol{Y}_{n1}$, $\boldsymbol{Y}_{n2}$ and $\boldsymbol{Y}_{n3}$ respectively. According to the node correspondence between the sub-network and the overall network, the elements of $\boldsymbol{Y}_{n1}$, $\boldsymbol{Y}_{n2}$ and $\boldsymbol{Y}_{n3}$ are mapped and superimposed on the corresponding nodes, and finally aggregated into the nodal admittance matrix of the complete network.

$$\mathbf{Y}_n = \mathbf{Y}_{n1} + \begin{bmatrix} \mathbf{Y}_{n2} & 0 \\ 0 & \mathbf{Y}_{n3} \end{bmatrix}. \tag{29}$$

4.4 *Calculation of frequency response curve*

Based on the establishment of the admittance matrix $\boldsymbol{Y}_n$ of the entire network nodes, the node voltage vector of the entire network can be calculated according to Equation (11). Then, according to the calculation principle of the frequency response method, select the node voltage of the response end of each phase high voltage winding and low voltage winding, and substitute it into Equation (1) to calculate the frequency response of each phase high voltage and low voltage winding in the equivalent circuit of the lumped parameter of the transformer winding. In IEEE Std C57.149-2024 [6], the connection requirements for FRA have been clearly given. According to this standard, taking the measurement of the frequency response of the high voltage A phase and the low voltage a phase winding as an example, draw the connection diagram of the three-phase lightning protection transformer winding with connection group Yzn11, as shown in Figure 8.

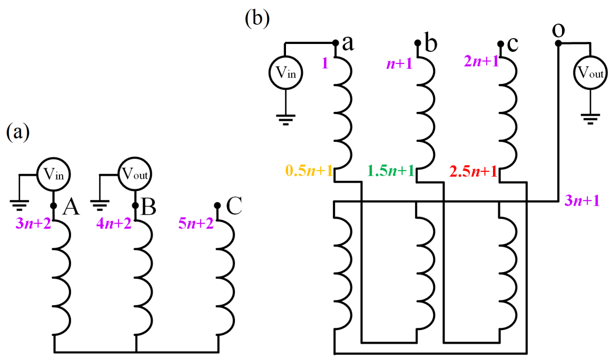

Figure 8. Yzn11 frequency response test connection diagram. (a) HV A-phase connection method; (b) LV A-phase connection method

In Figure 8, when calculating the frequency response of the high-voltage phase A winding, the input voltage signal enters from terminal A and exits from terminal B of the high-voltage winding; when calculating the frequency response of the low-voltage phase a winding, the input signal enters from terminal a and exits from terminal o of the neutral point. Similarly, the other phases are measured in the same way. The specific incentive and response terminals of each phase, as well as the node labels in the corresponding equivalent circuit, are shown in Table 1. According to the given incentive and response terminal node labels, the frequency response curves of each phase's high-voltage and low-voltage windings in the range of 1kHz to 1MHz can be calculated respectively.

Table 1. Node labels for excitation and response ends in frequency response calculation

Test winding	Incentive terminal	Response terminal
HV phase A	A：$3n + 2$	B：$4n + 2$
HV phase B	B：$4n + 2$	C：$5n + 2$
HV phase C	C：$5n + 2$	A：$3n + 2$
LV phase a	a：1	o：$3n + 1$
LV phase b	b：$n + 1$	o：$3n + 1$
LV phase c	c：$2n + 1$	o：$3n + 1$

Note: n is the number of discs.

5. Frequency response curve simulation verification based on PSpice

To verify the accuracy of the proposed method, two equivalent circuit models with different numbers of discs were constructed using the PSpice simulation platform. Frequency response calculations are performed, and amplitude-phase curves are obtained. Comparative verification confirmed the effectiveness of the proposed method. Figure 9 shows the calculation and simulation results of the FRA curves for the three-phase high and low voltage windings with 10 discs. It can be seen that the algorithm described in this paper and the FRA curves obtained using PSpice simulation software exhibit a high degree of consistency across the entire frequency range. Figure 10 shows the calculation and simulation results of the FRA curves for the three-phase high and low voltage windings with 20 discs. It is evident that the FRA curves obtained by the two methods also almost completely overlap across the entire frequency range.

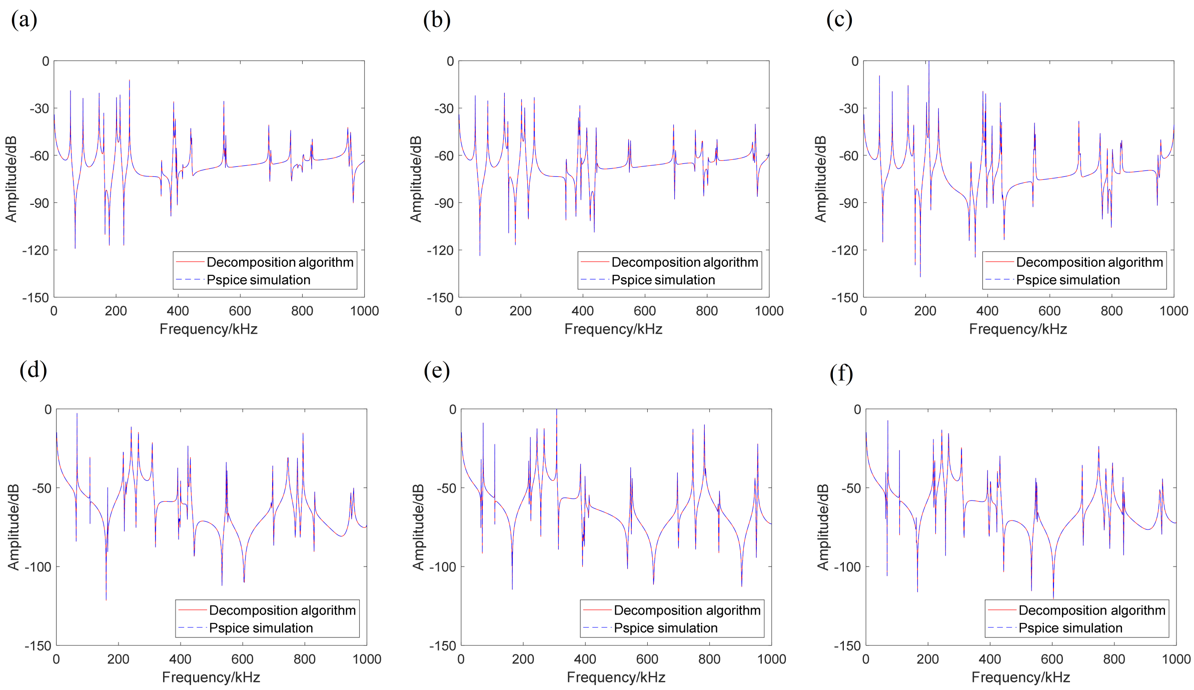

Figure 9. FRA curves comparison (10 discs). (a) HV phase A; (b) HV phase B; (c) HV phase C; (d) LV phase a; (e) LV phase b; (f) LV phase c

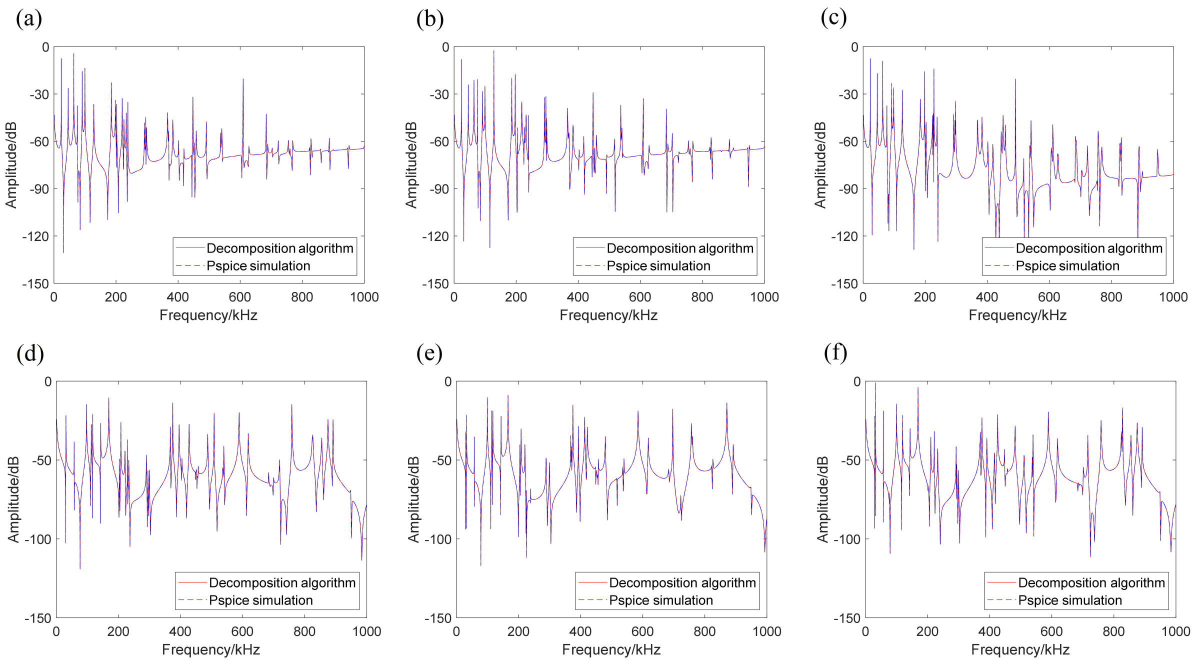

Figure 10. FRA curves comparison (20 discs). (a) HV phase A; (b) HV phase B; (c) HV phase C; (d) LV phase a; (e) LV phase b; (f) LV phase c

To objectively and quantitatively compare the differences between the calculation results of the two methods, this paper uses two numerical indicators, Correlation Coefficient (CC) [25] and Comparative Standard Deviation (CSD) [26], to quantitatively describe the consistency and difference between the FRA curves obtained by the method and the simulation by PSpice. CC is an indicator for analyzing the similarity between frequency response curves. The closer the value of this indicator is to 1, the more similar the two curves are. Its calculation formula is shown in Equation (30). CSD is a statistical indicator for measuring the degree of deviation between variables in a dataset. Its value range is not strictly limited, but the smaller its value, the smaller the degree of deviation between the data. Its calculation formula is shown in Equation (31). The results of the calculation of the two data indicators under two different parameter conditions are shown in Table 2.

$$\mathrm{CC} = \frac{\sum_{i=1}^{N} X(i)Y(i)}{\sqrt{\sum_{i=1}^{N}[X(i)]^2 \sum_{i=1}^{N}[Y(i)]^2}}, \tag{30}$$

$$\mathrm{CSD} = \sqrt{\frac{\sum_{i=1}^{N}\left[\left(Y(i)-\overline{Y}\right)-\left(X(i)-\overline{X}\right)\right]^2}{N-1}}, \tag{31}$$

where X and Y are the amplitude vectors of two sets of frequency response data, respectively. $X(i)$ and $Y(i)$ are the i-th elements of these vectors, respectively. $\overline{X}$ and $\overline{Y}$ are the average amplitudes of the two sets of frequency response curve data, respectively. N is the total number of samples.

As shown in Table 2, the CC values of all six sets of FRA curves calculated by the two methods are greater than 0.999, and some CC values are even equal to 1. In addition, the CSD values are all less than 0.7, very close to 0. The above data calculation results indicate that the FRA curves calculated by the two algorithms are almost completely identical. This also proves the correctness of the calculation results from the perspective of data indicators.

Table 2. Results of CC and CSD

Test winding	CC		CSD	
	10 discs	20 discs	10 discs	20 discs
HA	1.0000	1.0000	0.1616	0.1572
HB	0.9999	0.9998	0.4993	0.5024
HC	1.0000	0.9997	0.1852	0.6842
La	1.0000	0.9999	0.2525	0.4461
Lb	0.9998	0.9999	0.6545	0.3326
Lc	1.0000	1.0000	0.2198	0.2894

Note: HA, HB, and HC represent the high-voltage A, B, and C phases, respectively. La, Lb, and Lc represent the high- and low-voltage a, b, and c phases, respectively.

6. Comparison of computation time of the algorithm

To further demonstrate the superiority of the method in terms of computation time, this paper compares the method with the traditional node voltage method. Also, to ensure the accuracy of the computation time, the two methods use the same node and branch numbering order, and the computation time is shown in Table 3. It can be seen that when the number of discs is small, the computation time of the two methods is similar, but a decomposition algorithm still leads. At the same time, as the number of discs increases significantly, the advantage of a decomposition method in terms of computation time becomes more and more obvious. When the number of wires increases to 100, the computation time of a decomposition algorithm is reduced by 55.3% compared with the traditional node voltage method. Therefore, when considering the connection group and dealing with the transformer frequency response calculation problem with a large number of discs, a decomposition algorithm shows a significant advantage.

Table 3. Comparison of calculation time

Calculation time/s	discs			
	10	20	50	100
Decomposition algorithm	10.671	28.268	330.465	4390.911
Node voltage method	12.577	36.371	391.185	9820.865

7. Conclusion

This paper takes a typical Z-type lightning protection transformer with Yzn11 connection group as an example and proposes a decomposition algorithm suitable for calculating the frequency response of the equivalent circuit of the windings of Z-type transformers with special structures. Utilizing the ”decomposition-integration” approach, the entire network is divided into three uncoupled subnetworks, and the nodal admittance matrix and correlation matrix of each subnetwork are calculated separately. Finally, based on the relationship between the subnetworks and the entire network, the frequency response calculation method for the entire network is derived. The accuracy of the algorithm was verified using PSpice simulation software. The results show that the FRA curves calculated by the two algorithms almost completely overlap across the entire frequency range, with a correlation coefficient greater than 0.999 and a standard deviation less than 0.7. Furthermore, a comparison of the proposed method with the traditional nodal voltage algorithm in terms of computation time reveals that the proposed method has a significant advantage, and this advantage becomes increasingly apparent as the number of winding discs increases. When the number of winding coils increases to 100, the computation time is reduced by 55.3%.

This study provides an efficient tool for frequency response simulation calculation of the equivalent circuit of Z-type transformer windings with special structures, further enriching the theory of transformer winding simulation calculation and providing important basic support for subsequent transformer fault diagnosis technology based on the frequency response method.

Author contributions

Z.L.: Conceptualization, Methodology, Writing—Original Draft; B.Z.: Writing—Review & Editing, Validation; H.P.: Writing—Original Draft, Software; Z.Y.: Investigation, Software; S.W.: Validation, Writing—Original Draft, Supervision; J.L.: Validation.

Acknowledgment

The authors gratefully acknowledge the technical guidance and support provided by Qianjiang Electric Group Co., Ltd.

Conflicts of interest

The authors declare no competing financial interest.

References

[1] M. Shen, L. Ingratta, and G. Roberts, "Grounding transformer application, modeling, and simulation," In Proc. IEEE Power and Energy Society General Meeting, Pittsburgh, PA, USA, Jul. 20-24, 2008, pp. 1-8. https://doi.org/10.1109/pes.2008.4595995.

[2] K. Karthi, R. Radhakrishnan, J. M. Baskaran, and L. S. Titus, "Role of ZigZag transformer on neutral current reduction in three phase four wire power distribution system," In Proc. International Conference on Intelligent Computing, Instrumentation and Control Technologies, Kannur, India, Jul. 6-7, 2017, pp. 138-141. https://doi.org/10.1109/icicict1.2017.8342548.

[3] S. Wang, H. Zhang, S. Wang, H. Li, and D. Yuan, "Cumulative deformation analysis for transformer winding under short-circuit fault using magnetic–structural coupling model," *IEEE Transactions on Applied Superconductivity*, vol. 26, no. 7, pp. 1-5, 2016. https://doi.org/10.1109/tasc.2016.2584984.

[4] H. J. Zhang, S. H. Wang, and S. Wang, "Cumulative deformation analysis of transformer winding under short-circuit fault using 3-D FEM," In Proc. IEEE International Conference on Applied Superconductivity and Electromagnetic Devices, Shanghai, China, Nov. 20-23, 2015, pp. 370-371. https://doi.org/10.1109/asemd.2015.7453617.

[5] S. Wang, B. Zhu, H. Peng, J. Liu, and S. Wang, "A new data augmentation model for fault diagnosis of transformer windings under scarce fault data," *IET Electric Power Applications*, vol. 20, no. 1, p. e70140, 2026. https://doi.org/10.1049/elp2.70140.

[6] IEEE, "IEEE guide for the application and interpretation of frequency response analysis for oil-immersed transformers," in *IEEE Std C57.149-2024*. IEEE, pp. 1-55, 2025. https://doi.org/10.1109/ieeestd.2025.10907879.

[7] S. M. Al-Ameri, M. S. Kamarudin, M. F. M. Yousof, A. A. Salem, A. A. Siada, and M. I. Mosaad, "Interpretation of frequency response analysis for fault detection in power transformers," *Applied Sciences*, vol. 11, no. 7, p. 2923, 2021. https://doi.org/10.3390/app11072923.

[8] A. Amara, A. Gacemi, H. Houassine, and M. S. Chaouche, "A novel methodology for high-frequency lumped equivalent circuit of an isolated transformer winding construction based on frequency response analysis signal morphology interpretation," *IET Electric Power Applications*, vol. 15, no. 2, pp. 171-185, 2021. https://doi.org/10.1049/elp2.12013.

[9] P. Saji, A. Muhammed and V. V., "Estimating the effect of axial displacement on equivalent circuit parameters of transformer winding using finite element method," In Proc. IEEE 5th International Conference on Condition Assessment Techniques in Electrical Systems, Kottayam, India, Dec. 3-5, 2021, pp. 311-316. https://doi.org/10.1109/catcon52335.2021.9670500.

[10] M. H. Samimi and S. Tenbohlen, "FRA interpretation using numerical indices: state-of-the-art," *International Journal of Electrical Power & Energy Systems*, vol. 89, pp. 115-125, 2017. https://doi.org/10.1016/j.ijepes.2017.01.014.

[11] X. Zhao, C. Yao, A. Abu-Siada, and R. Liao, "High frequency electric circuit modeling for transformer frequency response analysis studies," *International Journal of Electrical Power & Energy Systems*, vol. 111, pp. 351-368, 2019. https://doi.org/10.1016/j.ijepes.2019.04.010.

[12] S. H. C. Nguyen and D. A. K. Pham, "An efficient method to calculate power transformers' frequency response from a state-space model," In Proc. International Symposium on Electrical and Electronics Engineering, Ho Chi Minh City, Vietnam, Oct. 19-20, 2023, pp. 167-172. https://doi.org/10.1109/isee59483.2023.10299819.

[13] S. Wang, Z. Yuan, and S. Wang, "The comparison of nodal voltage matrix and state space methods for calculating the FRA curve of the transformer winding," In Proc. International Conference on Advanced Electrical Equipment and Reliable Operation, Beijing, China, Oct. 15-17, 2021, pp. 1-4. https://doi.org/10.1109/aeero52475.2021.9708319.

[14] S. Wang, W. Wang, F. Xie, S. Qiu, and F. Yang, "Cut-set matrix methods for frequency response analysis curves of lumped parameter equivalent circuit model of three-winding power transformer," *International Journal of Circuit Theory and Applications*, vol. 52, no. 3, pp. 1518-1530, 2024. https://doi.org/10.1002/cta.3833.

[15] F. Ren, S. Ji, L. Zhu, Y. Liu, F. Yang, W. Lu, et al., "Matrix algorithm for ladder network frequency response analysis of double-winding power transformer," *Journal of Xi'an Jiaotong University*, vol. 52, no. 2, pp. 89-95, 2018. https://doi.org/10.7652/xjtuxb201802014.

[16] Z. Zhang, "Derivation of transformer winding equivalent circuit by employing the transfer function obtained from frequency response analysis data," *IET Electric Power Applications*, vol. 18, no. 7, pp. 826-840, 2024. https://doi.org/10.1049/elp2.12436.

[17] V. Atanasov and E. Mechkov, "Technical economic analysis concerning connection groups of distribution transformers in Bulgaria," In Proc. International Symposium on Electrical Apparatus and Technologies, Bourgas, Bulgaria, Jun. 2024, pp. 1-5. https://doi.org/10.1109/siela61056.2024.10637866.

[18] R. C. Dorf, *Circuits, Signals, and Speech and Image Processing*. CRC Press, 2018. https://doi.org/10.1201/9781420003086.

[19] R. Khalilisenobari and J. Sadeh, "A novel numerical index for assessing results of frequency response analysis (FRA): an experimental study on electrical machines," In Proc. North American Power Symposium, Tempe, AZ, USA, Apr. 11-13, 2021, pp. 1-6. https://doi.org/10.1109/naps50074.2021.9449826.

[20] B. A. Thango, "Six sigma-based frequency response analysis for power transformer winding deformation," *Applied Sciences*, vol. 15, no. 7, p. 3951, 2025. https://doi.org/10.3390/app15073951.

[21] N. Hashemnia, "Characterisation of power transformer frequency response signature using finite element analysis," Ph.D. dissertation, Curtin University, Perth, WA, Australia, 2014.

[22] C. K. Alexander and M. N. O. Sadiku, *Fundamentals of Electric Circuits*, 7th ed. New York: McGraw-Hill, 2021.

[23] S. Claeys, G. Deconinck, and F. Geth, "Decomposition of n-winding transformers for unbalanced optimal power flow," *IET Generation, Transmission & Distribution*, vol. 14, no. 24, pp. 5961-5969, 2020. https://doi.org/10.1049/iet-gtd.2020.0776.

[24] Z. Zhang, M. Mo, and C. Wu, "Three-phase distribution transformer connections modeling based on matrix operation method by phase-coordinates," *EURASIP Journal on Wireless Communications and Networking*, vol. 2021, no. 1, p. 66, 2021. https://doi.org/10.1186/s13638-021-01945-z.

[25] M. Tahir, S. Tenbohlen, and S. Miyazaki, "Analysis of statistical methods for assessment of power transformer frequency response measurements," *IEEE Transactions on Power Delivery*, vol. 36, no. 2, pp. 618-626, 2020. https://doi.org/10.1109/tpwrd.2020.2987205.

[26] S. Banaszak and W. Szoka, "Transformer frequency response analysis with the grouped indices method in end-to-end and capacitive inter-winding measurement configurations," *IEEE Transactions on Power Delivery*, vol. 35, no. 2, pp. 571-579, 2019. https://doi.org/10.1109/tpwrd.2019.2915570.